Quantifying Cellular Forces: Practical Considerations of Traction Force Microscopy for Dermal Fibroblasts

Abigail De La Pena,[1†] Marah Mukhtar,[2] Ryosuke Yokosawa,[1‡] Santiago Carrasquilla,[3§] and Chelsey S. Simmons[1,3,4]

[1]Department of Mechanical and Aerospace Engineering, [2]Department of Materials Science and Engineering, [3]J. Crayton Pruitt Department of Biomedical Engineering, [4]Division of Cardiovascular Medicine, University of Florida

[†]Current affiliation: Thermo Fisher Scientific, acdlp2@gmail.com
[‡]Current affiliation: Food and Drug Administration, ryosukeyokosawa@gmail.com
[§]Current affiliation: Carnegie Mellon University, scarrasq@andrew.cmu.edu

ABSTRACT

Traction force microscopy (TFM) is a well-established technique traditionally used by biophysicists to quantify the forces adherent biological cells exert on their microenvironment. As image processing software becomes increasingly user-friendly, TFM is being adopted by broader audiences to quantify contractility of (myo)fibroblasts. While many technical reviews of TFM's computational mechanics are available, this review focuses on practical experimental considerations for dermatology researchers new to cell mechanics and TFM who may wish to implement a higher throughput and less expensive alternative to collagen compaction assays. Here, we describe implementation of experimental methods, analysis using open source software, and troubleshooting of common issues to enable researchers to leverage TFM for their investigations into skin fibroblasts.

KEYWORDS: Mechanobiology, contractility, cross-correlation algorithms, smooth muscle actin

1. INTRODUCTION

Dermal cells generate traction forces on their surroundings to migrate, contract wounds, and maintain barrier function. Given the complexities of wound healing processes, functional assays to monitor these forces can be useful in preclinical development of new therapeutic strategies. Modulation of migration can accelerate wound healing, e.g. via epidermal growth factor (1), and cell migration relies heavily on mechanical forces (2). Mechanical force can also intensify scar formation (3), and small molecule modulation of cell contraction has reduced scarring in mouse models after incisions (4) and burns (5). Techniques to optically monitor cellular forces in vitro, collectively called traction force microscopy (TFM), are promising functional assays to investigate fundamental pathophysiology of dermatological disease and to support development and screening of potential therapies to modulate wound healing and scar formation via force generation.

As an optical microscopy-based technique, TFM does not involve specialized metrology tools nor direct contact with cells, enabling inexpensive implementation and simple incorporation into most experimental workflows. In addition, TFM can be implemented using less expensive materials at lower quantities than those typically used for collagen-compaction-based assays of fibroblast contractility (6). Collagen-based assays also confound measures of contractility with matrix degradation, matrix

production, and cell-cell interactions (7), rendering TFM a valuable and potentially high-content complement to other cellular and molecular techniques.

Harris et al. first described wrinkling of thin silicone sheets as a method for estimating forces of adherent cells and are credited with launching the field of TFM (8). When cells were seeded onto compliant substrates, the traction forces they applied to the surface caused the substrate to "wrinkle"; this semi-quantitative Substrate Wrinkling Assay (SWA) is described in detail in Section 2. Briefly, microscope images of adherent cells under desired control and experimental conditions or as they are migrating capture the extent of substrate wrinkling (Figure 1). A highly cited early utilization of SWA correlated increased alpha-smooth muscle actin expression with increased fibroblast contractility (9), which now defines a commonly accepted feature of myofibroblast activation. Quantification of precise cell forces using this method is complex (10-12), so image processing routines to quantify apparent wrinkles as a proxy for force are often preferred.

More precise methods to quantify cellular contractile force were pioneered by Dembo and Wang (13), who added small markers to measure continuous deformations of thick substrates. These thick substrates have since become the standard for quantitative TFM (qTFM) as detailed in Section 3, and comparisons and considerations for using both SWA and qTFM are summarized in Table 1. In qTFM, cells are plated on compliant hydrogels that have small fiducial markers such as fluorescent beads embedded. Microscope images of the markers while cells are attached are compared to images of the markers once cells are released, and the force required to create the observed displacements can be calculated using equations from mechanics and knowledge of substrate stiffness. qTFM can also be used for multicellular analyses, though this approach is most common for monolayer-forming cells like keratinocytes, as evidenced by applications of qTFM to keratinocyte colony formation (14,15), cytoskeletal and junction protein assembly (16,17), and migration (18,19). Ladoux and Mege (2) provide an exceptional review of mechanics in collective migration with extensive discussion of wound healing and relevance to dermatology.

For additional background reading on TFM broadly, we recommend exemplary reviews of its methods (20-22) and its computational algorithms (23-25). Techniques for three-dimensional TFM also have been developed (26-29), but we assume readers are interested in simple assays to complement their ongoing investigations so specialized 3D TFM is not discussed further. For discussion of methods to assess cell forces that require additional fabrication and metrology equipment, we direct the reader to excellent reviews of micropost arrays (30)(31), fluorescent stress tensors (32,33)-(24), and more (34).

1.1. Applications Of TFM To Dermal Fibroblasts

Since the invention of TFM in the 1980s, SWA has been used extensively to observe dermal fibroblast contractility and, specifically, myofibroblast activation (9,11,35,36). Recently, to investigate processes that may be modulated to reduce scarring, SWA has been used to assess dermal fibroblast contractility as a feature of myofibroblast activation under hypoxic conditions (37), in co-culture with platelets (38), and in regenerative African Spiny Mouse cells (39). While SWA is typically used to examine heterogeneous populations of near-confluent cells, it can also be used on single cells plated at low density (11,35). Custom SWA substrates have also been used to improve the throughput of individual cell measurements to elucidate the role of individual genes in accelerated wound healing (40). Since multicellular monolayers are often used with SWA, this technique is compatible with subsequent collection of cells and lysate or fixation and imaging in situ after wrinkling images are acquired.

Leveraging qTFM as a single cell assay, groups have identified biophysical parameters that correlate with chronological age using normal human dermal fibroblasts (41) and myofibroblast

subpopulations with varying levels of contractility using fibroblasts from patients with Dupuytren's disease (42). Researchers have also leveraged qTFM to investigate the role of calponin, an inhibitor of myosin ATPase, in non-muscle cell contractility (43), mechanisms of cobalt-induced fibrosis (44), and contractility of primary dermal fibroblasts from the regenerative African Spiny Mouse (39).

Two-dimensional TFM holds broad appeal for dermatology researchers interested in characterizing fibroblast contractility, but implementation requires mastery of substrate fabrication and image analysis. In this review, we detail the two most straightforward approaches to TFM – semi-quantitative SWA and qTFM – while focusing on practical experimental concerns for researchers new to the methods. Opportunities, challenges, and research questions well suited for these two methods are summarized in Table 1.

Table 1. Comparison of Common 2D Methods to Study Cell Contraction

Technique	Opportunities	Challenges	Ideal Research Questions
Substrate Wrinkling Assay (SWA)	• Simple substrate fabrication compatible with standard tissue culture plates, flasks, and dishes • Wrinkles can be detected with low magnification to accommodate heterogeneous populations • Straight-forward image processing • Can be paired with broad range of additional assays	• Surface modification of silicone requires some optimization of non-standard culture methods • Quantitation by image processing alone does not resolve force • Wrinkles are not stable under all fixation protocols	• **Gain/loss of function**, e.g., hypoxic conditions (37) or genetic manipulation (40) • **Rare or hard-to-obtain, e.g. patient-derived, cells** as easier technique likely to yield robust data with fewer attempts (39) • **Soluble factor** effects, e.g. dose response curves, since multicellular data can be rapidly obtained without an automated stage
Quantitative Traction Force Microscopy (qTFM)	• Traction forces can be resolved for individual cells • Cell-cell forces can be calculated among cell clusters and/or monolayers • Single-cell analysis enables characterization of heterogeneity within cell populations • Compatible with additional optical-microscopy-based assays	• Images must be paired; benefits from automated stage • Image processing and force calculations require numerous steps; programming skills required to automate • Chemical functionalization required to anchor gels to coverslips and protein coating to gels	• **Cell-cell adhesive forces** can be estimated from cell doublets or larger colonies (45,46), (47); cell adhesion can be controlled with patterns (48,49) • **Cell migration** can be quantified by local force and displacement vectors (41,50) • **Subcellular features** can be quantified precisely; adhesive regions can be patterned to control cell shape and localization of adhesions (51)

2. TECHNICAL DETAILS OF SUBSTRATE WRINKLING ASSAY

2.1. Overview of SWA Workflow

Compliant silicone substrates are crosslinked onto tissue culture plastic or glass for analysis of cell contractility. Substrate surfaces are functionalized with plasma or chemical treatments, sterilized with UV or ethanol, and matrix-coated in preparation for cell plating. Then, cells are seeded on the substrate and allowed to grow to the required confluency. Next, microscope images are taken of adhered cells under desired control and experimental conditions to capture substrate wrinkling (Figure 1). Images can be processed to quantitate the number and/or size of wrinkles.

2.2. Substrate preparation for SWA

Polydimethylsiloxane (PDMS), a type of silicone, is prevalent in microfluidic devices and commonly used as a soft substrate for cell culture. PDMS is prepared according to manufacturer's instructions (e.g. Sylgard 527, Dow Corning) by combining two components in disposable cups with disposable mixing sticks for ease of cleaning. Viscous prepolymer solution will stick to mixing vessel, so it is recommended to mix ~30% more than the desired final volume. The silicone mixture can be poured into 6-well plates, petri dishes, or the bottom of flasks, desiccated under vacuum for 1 hour, and allowed to cure at 70°C overnight. Silicone substrates can be fabricated in a wide range of stiffnesses to mimic various tissues and pathologies by mixing silicones (52) or ready-to-use substrates purchased commercially, e.g. Excellness Biotech (Lausanne, Switzerland) and Advanced BioMatrix (San Diego, CA). Substrates with a modulus less than 10 kPa are recommended for basic SWA; stiffer substrates yield few wrinkles.

The high surface hydrophobicity of PDMS limits cells adhesion to bare PDMS, so surface treatment is recommended. Oxygen plasma (e.g. Harrick Plasma or ozone sterilization) and covalently bonded chemicals can improve cell attachment and spreading compared to unmodified PDMS (79), but chemical functionalization can be time-intensive and autofluorescence of chemicals can interfere with immunofluorescence microscopy. Coating with charged molecules like poly-lysine or proteins like collagen I can also enhance attachment, though the choice of matrix protein affects contractility (53).

2.3. Cell Culture and Image Acquisition

Cells are seeded on silicone substrates at the desired density. At confluency or other desired timepoint, phase-contrast images of the adhered cells are acquired for quantification of wrinkles. Since SWA images can be obtained at low magnification in standard culture plates, additional experimental factors can be assessed. For example, contractility can be quantified before and after being treated with Blebbistatin, a myosin inhibitor that induces cell relaxation as in Supplemental Figure I. Alternatively, after imaging, cells could be lysed for analysis or fixed for immunostaining.

2.4. Quantifying Wrinkles via Image Processing

Quantification of substrate wrinkling can be done by hand, semi-automated, or fully automated (see discussion in Supplemental Files). Briefly, ImageJ (NIH) can be used to trace each wrinkle and measure the traced area. Because this method is time-intensive, it is recommended only for small samples sizes or images with high background noise. Alternatively, users can set a threshold for each image and the resulting highlighted wrinkles are automatically calculated. This semi-automatic approach is useful for large data sets, though a blinded approach or analysis by duplicate researchers is recommended to mitigate bias. A fully automated macro for this process can be written in ImageJ or MATLAB (Mathworks), but it is difficult to set universal thresholding parameters. Human users can

compensate for noise from image to image, but setting an appropriate parameter in the code that automatically works for all images has proven difficult.

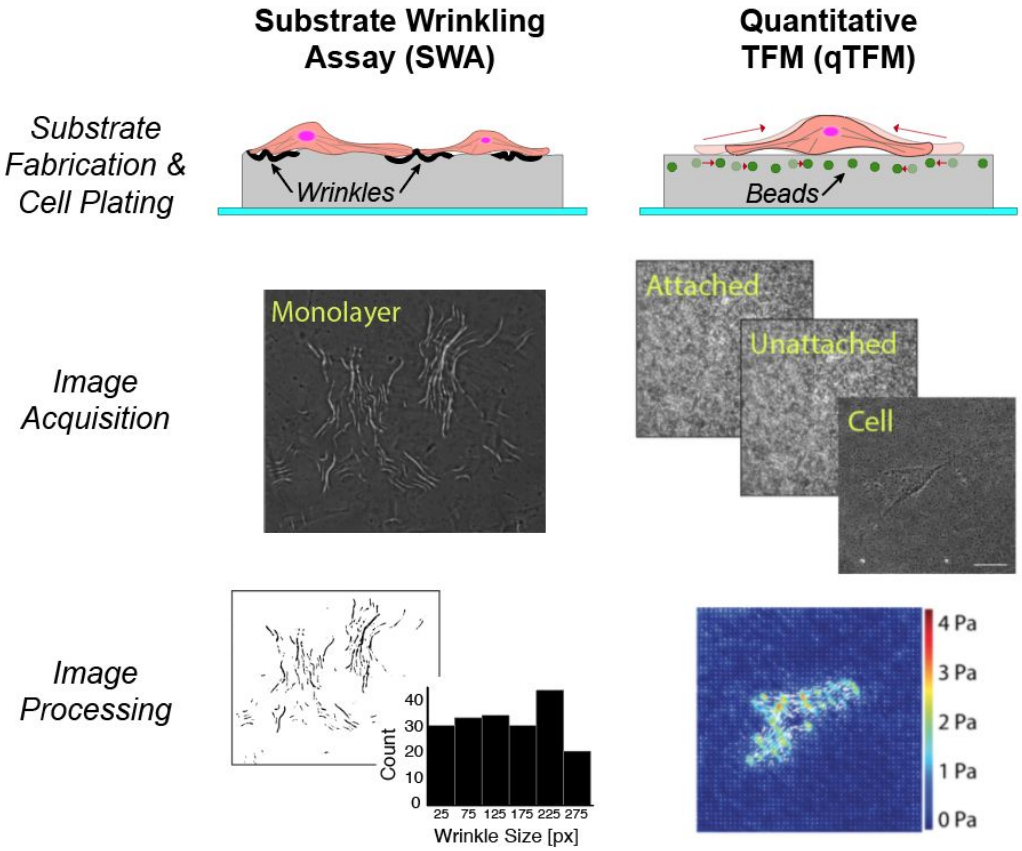

Figure 1. Simple procedures to assay contractility in dermal fibroblasts. In both assays, specialized culture substrates are prepared for cell plating. For the semi-quantitative substrate wrinkling assay (SWA), phase-contrast images of the plated cell monolayer can be processed to quantitate the number of "wrinkled" pixels. For quantitative TFM (qTFM), a substrate with fluorescent markers (e.g., beads) is fabricated and functionalized to support cell attachment. A phase or brightfield image of the cell is acquired to determine cell boundary, and then a fluorescence image of fiducial markers with the cell "attached" is acquired. Additional images can be acquired of live cells to monitor changing environmental conditions and/or migration. An "unattached", a.k.a. "null", fluorescence image of fiducial markers after removing the cell(s) is then acquired for post-processing to calculate traction forces. The resulting strain energy and/or a heat map of cell stresses are output by various algorithms. Additional details in text.

3. TECHNICAL DETAILS OF QUANTITATIVE TRACTION FORCE MICROSCOPY

3.1. Overview of qTFM Workflow

Cell-induced deformations of hydrogels are quantified by processing images of fiducial markers, e.g., fluorescent beads, embedded in the gel. After fabrication, the substrate is characterized to determine mechanical properties and functionalized with chemicals and matrix proteins to ensure cell attachment. Next, microscope images are taken of the beads underneath cells in control and treatment conditions; afterward, cells are removed to capture the beads in an unstressed state for comparison (Figure 1). Some form of image registration using an automated stage, additional fiducial markers, and/or meticulous manual location-finding is necessary to compare reference and experimental images. After computing a

displacement field for the beads, cell traction forces can be quantified using continuum mechanics implemented through a variety of algorithms (24).

3.2. Substrate Preparation for qTFM

3.2.1. Substrate Fabrication. The two most common materials used in qTFM are polyacrylamide (PAA), a polymer made out of repeating acrylamide subunits, and silicone, the same PDMS polymer used for SWA. PAA is readily available in most biomedical labs and is easier to decorate with fiducial markers than PDMS, so it is used more often for qTFM and will be discussed in detail here. PAA also affords negligible surface adsorption of serum proteins compared to PDMS but swells if not osmotically balanced. Mechanical properties of PAA (i.e. elastic moduli) can be tuned from ~100 Pa to 100 kPa by adjusting the acrylamide monomer and bisacrylamide crosslinker ratio (54-61). For more detail, Tse and Engler have published step-by-step protocols for the fabrication of various PAA hydrogel formulations with their respective elastic moduli (61).

Since mechanical properties like elastic modulus are used during computational analysis to calculate forces or stresses (62,63), the PAA substrate must be well characterized. However, mechanical characterization of PAA gels can yield dramatically different values depending on the fabrication method, characterization method, age, and hydration of the gels (64). Researchers are encouraged to characterize under experimental conditions to ensure accurate values for analysis. If access to mechanical characterization equipment is limited, the reader is directed to Bashirzadeh et al. which details characterization using microscopy and inexpensive steel ball bearings (65).

3.2.2. Integrating Fluorescent Markers. Fiducial markers, typically fluorescent polystyrene beads with diameters 0.5-2 μm that can be imaged at 200-400x total magnification, are needed to track deformation of the substrate and quantify forces exerted by cells. Several methods have been developed to incorporate beads to the substrate, and the method used can greatly affect signal-to-noise ratio (SNR, see discussion in Supplemental Files). Emerging advanced manufacturing techniques enable sophisticated patterning of markers (39,40), but the simplest method to incorporate fiducial markers remains to mix the pre-polymer solution with fluorescent beads and polymerize the hydrogel following normal protocols. Alternatively, conjugation of functionalized beads to the top surface of the substrate can reduce background fluorescence from out-of-focus beads and increase the SNR (66). Matrigen, LLC (Brea, CA, USA) offers PAA substrates with embedded beads as a custom order. Alternatively, silicone substrates for quantifying single-cell contractions are available from Forcyte Biotechnologies Inc. (Los Angeles, CA, USA); their platform includes an ‘x’ shaped pattern (67) and the change in size of the ‘x’ can be used to estimate forces and bypass the computations described in section 3.4.

3.2.3. Functionalization and Protein Coating. PAA gels do not naturally facilitate the adsorption of protein; therefore, they must be functionalized to allow proteins to attach to the substrate and allow cell adhesion. The most widely-used chemical to functionalize PAA is N-sulfosuccinimidyl-6-(4’-azido-2’-nitrophenylamino) hexanoate (sulfo-SANPAH) (61,68). A typical protocol is to pipette 1mM of sulfo-SANPAH in 50 mM HEPES buffer (pH 8.5) over the PAA gel and then expose it to UV-A light for 3 to 15 minutes. The sulfo-SANPAH is aspirated carefully by tilting the plate so as not to damage the gel, and the gels are rinsed at least thrice with a saline solution, typically PBS or HEPES. These steps may be repeated to facilitate better protein attachment. Functionalization will depend highly on peak wavelength emission of the UV chamber, distance between sample and UV source, and concentration of sulfo-SANPAH over the PAA gel. *Note:* Germicidal UV (as in a biosafety cabinet) is UV-C and will not work to activate sulfo-SANPAH, so a separate high-wattage UV-A source is needed. Alternatively, activation of PAA can be achieved by functionalizing acrylamide with reactive end-groups before polymerization (69-71).

After functionalization, matrix proteins can be pooled on the surface at concentrations between 10-100 µg/ml for incubation times ranging from 30 mins at 37°C to overnight at 4°C. Generally, small volumes with high concentrations of protein are easier to keep localized on the gel surface. A reasonable initial protocol could utilize volumes and concentrations that yield ~40 ng/mm^2 on the gel surface, assuming all protein came out of solution and attached, and to allow incubation for 2 hr at 37°C. Alternatively, microcontact printing (72) or microarrayed spots (73) can control shape and size of cell attachment regions. A simple way to test functionalization is by coating the activated hydrogel with an ECM protein conjugated with a fluorescent marker, e.g. inexpensive Protein A-FITC. Traditional immunostaining with antibodies can also test attachment and patterns (59).

After functionalization and protein coating, moderate to high concentrations of suspended cells (e.g. 10,000 cells/cm^2) are pooled on the gel in small volumes for a short period (10-20 mins) to facilitate attachment of cells to regions of interest. Additional media is added to dilute and clear cells that have not landed on areas of interest and to facilitate further attachment and spreading of remaining cells for hours or days, as desired.

3.3. Image Acquisition and Pre-Processing

3.3.1. Acquisition Parameters and Maintaining Precise Focal Plane. Image acquisition of the fiducial markers and preparation of the images for analysis is a critical step in TFM, as any irregularities acquired will be amplified in subsequent processing which will limit interpretation of results. To get accurate displacement vectors from the bead displacement, sharp images of the fluorescent beads on the cell-substrate interface are required. Out-of-focus beads induce erroneous vectors that increase noise and can result in detection of strain energy that does not correspond to the force generation of the cell (Supplemental Figure IV). Flatness of the culture surface and subsequent focal plane of the beads is particularly susceptible to poor fabrication technique, details of which are discussed in Supplemental Files.

The focus of the image is affected by how much light is refracted when it passes through the media, the cell, the hydrogel construct, and the lens. It is therefore recommended to use clear hydrogels and limit the thickness of the substrate to <200 µm; however, thickness should be >>10 µm, so that cells cannot sense underlying rigid substrates (74). Ideally, each image taken will be manually focused at each time point; however, this is time-consuming and some motorized stages enable automation of image acquisition. Furthermore, changes in media levels (i.e. from removal, addition, or evaporation of media) and potentially temperature variations can result in small changes to the focal plane. Small drifts in z-plane focus can substantially affect the accuracy of subsequent algorithms. For our setup using <1 µm-diameter beads and 200x magnification, we found a 13% error while 2 µm out-of-focus (Supplemental Figure IV). Strategies to reduce out-of-focus error and additional discussion of biological considerations for time-lapse experiments are included in Supplemental Files.

3.3.2. Stack Alignment. Stage drifting is common in motorized stages, especially when performing long time-lapse experiments, or when the plate must be removed from the stage, e.g. to add soluble factors. In addition to experimental controls, digital algorithms can improve alignment of a given set of images. For high-content experiments, i.e. >100 images, additional fabrication steps can support rapid stack alignment with a second reference layer of beads (15,75) or a regularized grid (76). The *Template Matching* ImageJ plugin at https://sites.google.com/site/qingzongtseng/template-matching-ij-plugin rapidly aligns a stack of images using one of six matching algorithms; however, it requires the user to select a reference region with minimal deformation. Alternatively, *Linear Stack Alignment with SIFT* (included with ImageJ/Fiji at https://fiji.sc) does not require manual input from the user but takes longer (77).

3.4. Displacement Quantification Using Cross-Correlation

Before force calculations, qTFM requires calculation of displacement fields of the fluorescent beads (Figure 2A-C). This can be achieved by particle tracking, correlation-based tracking, or a hybrid of both techniques; see detailed comparison in Holenstein et al. (78). Correlation-based methods have short computational times and are widely available, so this section will review their practical implementation to quantify substrate displacements. Additional discussion and comprehensive details of correlation tracking algorithms can be found in Supplemental Files and Raffel et al. (79), respectively.

3.4.1. Software Package Selection. There are numerous cross-correlation algorithms and implementations available for particle tracking across an international community (see, for example, http://www.pivchallenge.org/). We recommend a user-friendly open-source platform developed by Thielicke and Stamhuis called *PIVlab* that works as a MATLAB (MathWorks) dependency (80,81). *PIVlab* simplifies the input of images and setting parameters to get the displacement of the fluorescent particles. Academic licenses for MATLAB are inexpensive and most universities (especially engineering departments) maintain site licenses; downloads and several tutorials for *PIVlab* can be found at http://pivlab.blogspot.com/. *PIVlab* allows two different correlation algorithms; the Fourier-transform-based correlation (labeled "FFT") is recommended as it can reduce computation time by ~1000-fold. *PIVlab* also provides several pre-processing techniques for image enhancement to improve the quality of calculated displacements (Supplemental Files). In addition to digital enhancement, the region of interest ("ROI") feature in *PIVlab* can be used to ignore debris or dark spots that would affect calculations.

Another user-friendly implementation is the ImageJ plugin *PIV* by Tseng found at https://sites.google.com/site/qingzongtseng/piv (82). The "iterative PIV(Cross-correlation)" menu option is recommended as a starting point as it requires the least user input. Thorough guidance on utilizing ImageJ for qTFM and optimizing parameters for each step of analysis have been compiled by Martiel et al. (83).

3.4.2. Interrogation Region Size. The interrogation region (IR) selected for the different passes of Fourier-based algorithms of *PIVlab* and *PIV* will impact vector resolution and SNR. IR defines the size (usually in pixels) of the region to be compared from frame to frame (79,81). The choice of IR is informed by the size, distribution, and concentration of fiducial markers as well as the magnification of image acquisition (Figure 2D,E). The length of the IR should be equal to 2^n pixels, and this length should be greater than twice the marker displacements to avoid aliasing during Fourier-based computations. For example, if the maximum bead movement is 20 pixels, then the IR should be greater than 40 pixels. Bead size and distribution should be balanced with image magnification so that more than 5 beads are always in each IR to provide acceptable SNR (as determined by simulations; see Raffel et al. (79)).

Larger IRs for a set magnification and bead size will include more beads and thus better SNR; however, larger IRs decrease the spatial resolution of displacements and thus force vectors. Beginning analysis with an inappropriately small IR, i.e. a similar length to expected displacements, is also hazardous as beads may "disappear" between frames as they move to an adjacent IR and cause erroneous displacement vectors. Some algorithms, including *PIVlab* and *PIV*, enable multiple passes of successively smaller IR size to mitigate this conflict. Since each pass is fed information from previous passes, users can begin with a relatively large IR and still end up with good spatial resolution after 2-3 passes. As an example from our previous work, *PIVlab* was used to generate displacement fields using two passes with an IR of 128 px and 64 px for the first and second pass, respectively, with a 50% step size at 200X magnification (image resolution of 0.16 μm/px with 0.52 μm diameter beads) (84). The

default settings in *PIV*, i.e. three passes with decreasing IR sizes of 128, 64, and 32 px, are reasonable for most single-cell images. However, if your magnification and density of beads suggest IRs > 32 px, you may choose to skip the third pass by setting the input value to "0".

3.4.3. Post-Processing. *PIVlab* and *PIV* also include "vector validation" features to diminish erroneous vectors resulting from poorly distributed beads, under/overexposure, debris, and/or IRs on the image periphery. Empirically, in *PIVlab*, we found replacing vectors over 5 standard deviations from the mean with a vector average of adjacent IRs retains reasonable displacements while eliminating the most obvious erroneous vectors. *PIV* allows users to iteratively test two different post-processing methods, restore original results, or accept output and save. If numerous erroneous vectors are appearing at image edges, systematic cropping of stack-aligned images can reduce noise from peripheral regions. Cropping the image, for example, can help reduce noise from areas where no displacements should be detected. The exact dimensions of the cropped region could be adjusted to fulfill different cell morphologies, but multiples of IR edge length are recommended, i.e., length = A x 2n and width = B x 2n.

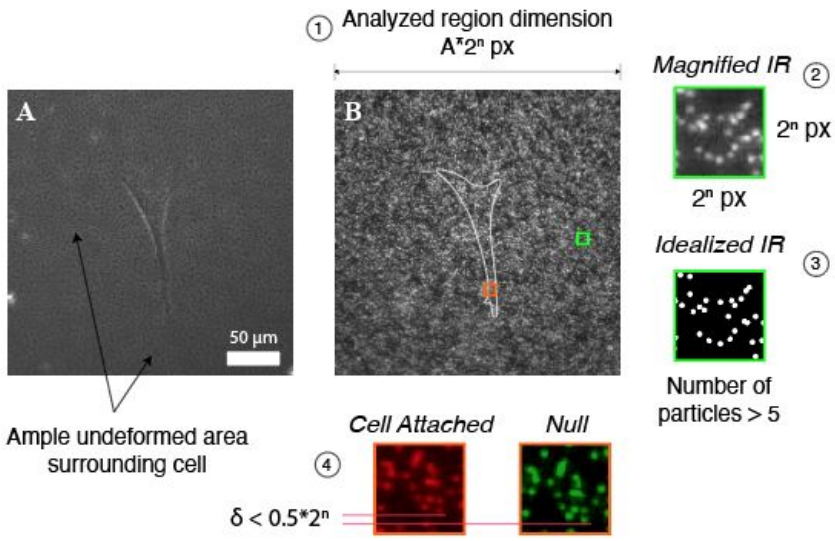

Figure 2. Schematic illustrating critical dimensions for image acquisition and processing for single cell TFM. Phase-contrast image (A) of smooth muscle cell on 45 kPa polyacrylamide gel illustrates undeformed perimeter roughly half cell length to support single-cell analysis. Fluorescence image of bead layer (B) highlights features critical for correlation algorithms including (1) overall dimensions that are a multiple of the interrogation region (IR) dimensions, (2) IR dimensions which should be 2^n pixels for subsequent Fourier-based analysis, (3) more than five particles per IR, and (4) particle displacements less than half the IR dimension. See Raffel et al. (79) for additional details.

3.5. Calculating Traction Forces, Stresses, and Energy

3.5.1. Primer on Mechanics Terminology and Units. After calculating displacements, vectors must be converted to forces. The simplest constitutive model relating displacement to force is Hooke's Law, $F = kx$, where F = force (units: Newtons, N), k = spring stiffness (units: N/m), and x = displacement (units: m). Using engineering stress and engineering strain, Hooke's Law for linear elastic materials can be written as $\sigma = E\varepsilon$, where σ = stress (force/area, units: Pascals, Pa = N/m^2), E = Young's Modulus (units: Pa), and ε = strain (change in length/original length, units: typically %).

Different algorithms quantify different measures of contractility, and distinguishing among them is important to compare across algorithms and experiments. Some approaches estimate force directly, while others calculate force distribution over an area (stress). Reported forces and stresses are often displayed as a heat map and statistics performed on maximum or average force or stress magnitude. Alternatively, statistics are performed on strain energy, which describes contractility as the total energy transferred from the cell to the substrate (units: Joules, J; see below). Therefore, care should be taken to report force, stress, and energy correctly according to algorithms employed.

3.5.2. Calculating Contractility. There are numerous algorithms to calculate force, stress, and/or strain energy from bead displacement data; see technical discussion in Schwarz and Soiné (24). However, algorithms relying on the common assumption that bead deformations are small perform analogously (23), so we recommend Fourier Transform Traction Cytometry (FTTC) (50,60) because it does not require a cell outline and has the fastest processing time. The FTTC algorithm can be implemented in MATLAB to utilize displacements output by *PIVlab* or other cross-correlation applications.

Alternatively, an ImageJ plugin that utilizes the FTTC algorithm to calculate cellular stresses is freely available at https://sites.google.com/site/qingzongtseng/tfm. Conveniently called *FTTC*, this plugin reads in the output of *PIV* and, together with user input, produces a visual display and text file of traction vectors. Likely because of historical quirks of vocabulary in the field, traction "forces" are output in units of stress (Pa). When using this program, we recommend either referring to output results (likely in kPa range) as "traction stresses" or converting to forces by multiplying by the IR area in μm^2 (likely yielding values in µN range) to avoid further confusion.

To generate a representative value to describe cell contractility that is useful for statistical analyses, strain energy, W, or the equivalent work that the cell had to perform to deform the substrate, can be calculated. Recommendations for implementing this calculation using ImageJ-based *PIV* and *FTTC* results are in the Supplemental Files.

4. SUMMARY

Functional assays of cell contractility remain critical to understanding skin remodeling, repair, and regeneration. TFM is a powerful functional assay to simply and inexpensively quantify fibroblast contractility and complement traditional cellular and molecular assays. Common sources of variability and suggestions for mitigating misleading analyses are summarized in Table 2. For researchers new to functional biophysical assays, SWA is recommended for its ease of fabrication and streamlined post-processing. SWA has been widely used to investigate changes in contractility with environmental, genetic, and pharmacological variables. For single-cell investigations, qTFM has become preferred as it provides more precise subcellular information. With increasingly straightforward software and commercially available substrates, these TFM techniques can now be added to the toolbox of any laboratory for quantitative insight into cell contractility.

Table 2. Trouble-Shooting Traction Force Microscopy

Concern	Mitigation Strategies
Poor cell attachment, cell death	**Improve protein attachment:** higher concentrations of functionalization chemicals and/or proteins; increased wash steps and/or wash times (SWA: §2.2, qTFM: §3.2.3) **Improve environmental control:** increase temperature and/or time for protein and cell attachment; reduce exposure time/intensity of fluorescence exposure; adjust media formulation (Supplemental Files §B.2)
Suspicious wrinkle counts (SWA)	**Improve signal-to-noise ratio:** Reduce hydrogel stiffness (§2.2); crop images and/or use regions-of-interest to exclude errant regions **Leverage computational tools:** Consider different analytical approaches (Supplemental Files §A); exclude wrinkles likely to represent noise (e.g. less than 4 px^2 in area) and/or overexposed regions (e.g. greater than reasonable size determined by observation)
Randomly oriented	**Improve signal-to-noise ratio:** optimize fabrication of gels to ensure level and well-distributed field of markers (Supplemental Files §B.1); enhance image focus (Supplemental Files §B.3); reduce hydrogel stiffness (§3.2.1); reduce size of IR (§3.4.2)

displacement vectors (qTFM)	**Leverage computational tools:** crop images and/or use regions-of-interest to exclude errant regions; pre-process images (Supplemental Files §B.4); pre-align images before calculating displacements (§3.3.2); apply vector validation or ensemble average to smooth vectors (§3.4.3)
Suspicious force values (qTFM)	**Check units:** ensure displacements, forces (e.g. N), and stresses (e.g. Pa = N/m^2) are all converted correctly from pixels with appropriate orders of magnitude (§3.5) **Improve cell health:** see recommendations above **Inspect displacement data:** poorly adhered cells, stiff substrates, and large interrogation regions (IRs) could lead to displacement quantification near the noise floor and subsequently lower-than-expected forces; randomly assigned vectors can result from regions that have no beads or beads that move out of frame can result in higher-than-expected forces, so ensure beads are well distributed (§3.2.2), consider increasing size of IR (§4.3.2), and/or implement vector validation (§3.4.3) **Reconsider microscopy parameters:** increasing optical (not digital) magnification and/or improving resolution of acquired images will enable additional passes with smaller IRs and potentially better resolution of localized displacements and forces

SWA = Substrate Wrinkling Assay; qTFM = Quantitative Traction Force Microscopy

ACKNOWLEDGEMENTS

We thank Dr. John M. Maloney for editorial assistance. This material is based upon work supported in part by the National Science Foundation (1636007) and the National Institute for General Medical Sciences of the National Institutes of Health (R35GM128831). The content is solely the responsibility of the authors and does not necessarily represent the official views of the funding agencies.

REFERENCES

1 Öhnstedt E, Tomenius H L, Vågesjö E *et al.* The discovery and development of topical medicines for wound healing. Expert Opinion on Drug Discovery 2019: **14**: 485–497.

2 Ladoux B, Mège R-M. Mechanobiology of collective cell behaviours. Nat Rev Mol Cell Biol 2017: : 1–16.

3 Duscher D, Maan Z N, Wong V W *et al.* Mechanotransduction and fibrosis. Journal of Biomechanics 2014: **47**: 1997–2005.

4 Wong V W, Rustad K C, Akaishi S *et al.* Focal adhesion kinase links mechanical force to skin fibrosis via inflammatory signaling. Nat Med 2012: **18**: 148–152.

5 Ma K, Kwon S H, Padmanabhan J *et al.* Controlled Delivery of a Focal Adhesion Kinase Inhibitor Results in Accelerated Wound Closure with Decreased Scar Formation. J Invest Dermatol 2018: **138**: 2452–2460.

6 Tomasek J J, Gabbiani G, Hinz B *et al.* Myofibroblasts and mechano-regulation of connective tissue remodelling. Nature Reviews Molecular Cell Biology 2002: **3**: 349–363.

7 Brown R A. In the beginning there were soft collagen-cell gels: towards better 3D connective tissue models? Experimental cell research 2013: **319**: 2460–2469.

8 Harris A K, Wild P, Stopak D. Silicone rubber substrata: a new wrinkle in the study of cell locomotion. Science 1980: **208**: 177–179.

9 Hinz B, Celetta G, Tomasek J J *et al.* Alpha-Smooth Muscle Actin Expression Upregulates Fibroblast Contractile Activity. MBoC 2001: **12**: 2730–2741.

10 Lee J, Leonard M, Oliver T *et al.* Traction forces generated by locomoting keratocytes. Journal of Cell Biology 1994: **127**: 1957–1964.

11 Fray T R, Molloy J E, Armitage M P *et al.* Quantification of single human dermal fibroblast contraction. Tissue Eng 1998: **4**: 281–291.

12 Yu X, Cross M, Liu C *et al.* Measurement of the traction force of biological cells by digital holography. Biomed Opt Express 2012: **3**: 153–159.

13 Dembo M, Wang Y L. Stresses at the cell-to-substrate interface during locomotion of fibroblasts. Biophysical Journal 1999: **76**: 2307–2316.

14 Zarkoob H, Bodduluri S, Ponnaluri S V *et al.* Substrate Stiffness Affects Human Keratinocyte Colony Formation. Cel Mol Bioeng 2015: **8**: 32–50.

15 Mertz A F, Banerjee S, Che Y *et al.* Scaling of Traction Forces with the Size of Cohesive Cell Colonies. Physical Review Letters 2012: **108**: 198101.

16 Rübsam M, Mertz A F, Kubo A *et al.* E-cadherin integrates mechanotransduction and EGFR signaling to control junctional tissue polarization and tight junction positioning. Nat Comms 2017: : 1–15.

17 Zarkoob H, Chinnathambi S, Halberg S A *et al.* Mouse Keratinocytes Without Keratin Intermediate Filaments Demonstrate Substrate Stiffness Dependent Behaviors. Cel Mol Bioeng 2018: **11**: 163–174.

18 Zarkoob H, Chinnathambi S, Selby J C *et al.* Substrate deformations induce directed keratinocyte migration. Journal of The Royal Society Interface 2018: **15**: 20180133–11.

19 Hiroyasu S, Colburn Z T, Jones J C R. A hemidesmosomal protein regulates actin dynamics and traction forces in motile keratinocytes. Faseb J 2016: **30**: 2298–2310.

20 Style R W, Boltyanskiy R, German G K *et al.* Traction force microscopy in physics and biology. Soft Matter 2014: **10**: 4047–4055.

21 Polacheck W J, Chen C S. Measuring cell-generated forces: a guide to the available tools. Nature Methods 2016: **13**: 415–423.

22 Roca-Cusachs P, Conte V, Trepat X. Quantifying forces in cell biology. Nature cell biology 2017: **19**: 742–751.

23 Sabass B, Gardel M, Waterman C *et al.* High resolution traction force microscopy based on experimental and computational advances. Biophys J 2008: **94**: 207–220.

24 Schwarz U S, Soiné J R D. Traction force microscopy on soft elastic substrates: A guide to recent computational advances. BBA - Molecular Cell Research 2015: **1853**: 3095–3104.

25 Mulligan J A, Bordeleau F, Reinhart-King C A *et al.* Traction force microscopy for noninvasive imaging of cell forces. In: Traction Force Microscopy for Noninvasive Imaging of Cell Forces. 2018: 319–349.

26 Franck C, Maskarinec S A, Tirrell D A *et al.* Three-Dimensional Traction Force Microscopy: A New Tool for Quantifying Cell-Matrix Interactions. PLoS ONE 2011: **6**: e17833.

27 Legant W R, Miller J S, Blakely B L *et al.* Measurement of mechanical tractions exerted by cells in three-dimensional matrices. Nature Methods 2010: **7**: 969–971.

28 Hall M S, Long R, Feng X *et al.* Toward single cell traction microscopy within 3D collagen matrices. Experimental cell research 2013: **319**: 2396–2408.

29 Toyjanova J, Bar-Kochba E, López-Fagundo C *et al.* High Resolution, Large Deformation 3D Traction Force Microscopy. PLoS ONE 2014: **9**: e90976.

30 Tan J, Tien J, Pirone D *et al.* Cells lying on a bed of microneedles: An approach to isolate mechanical force. Proceedings of the National Academy of Sciences of the United States of America 2003: **100**: 1484–1489.

31 Ribeiro A J S, Denisin A K, Wilson R E *et al.* For whom the cells pull: Hydrogel and micropost devices for measuring traction forces. Methods 2016: **94**: 51–64.

32 Cost A-L, Ringer P, Chrostek-Grashoff A *et al.* How to Measure Molecular Forces in Cells: A Guide to Evaluating Genetically-Encoded FRET-Based Tension Sensors. Cel Mol Bioeng 2015: **8**: 96–105.

33 Brockman J M, Blanchard A T, Pui-Yan V *et al.* Mapping the 3D orientation of piconewton integrin traction forces. Nature Methods 2018: **15**: 115–118.

34 Van Vliet K, Bao G, Suresh S. The biomechanics toolbox: experimental approaches for living cells and biomolecules. Acta Materialia 2003: **51**: 5881–5905.

35 Wrobel L K, Fray T R, Molloy J E *et al.* Contractility of single human dermal myofibroblasts and fibroblasts. Cell Motil Cytoskeleton 2002: **52**: 82–90.

36 Boswell C A, Majno G, Joris I *et al.* Acute endothelial cell contraction in vitro: A comparison with vascular smooth muscle cells and fibroblasts. Microvascular research 1992: **43**: 178–191.

37 Modarressi A, Pietramaggiori G, Godbout C *et al.* Hypoxia impairs skin myofibroblast differentiation and function. J Invest Dermatol 2010: **130**: 2818–2827.

38 Scherer S S, Tobalem M, Vigato E *et al.* Nonactivated versus Thrombin-Activated Platelets on Wound Healing and Fibroblast-to-Myofibroblast Differentiation In Vivo and In Vitro. Plastic and Reconstructive Surgery 2012: **129**: 46e–54e.

39 Stewart D C, Serrano P N, Rubiano A *et al.* Unique behavior of dermal cells from regenerative mammal, the African Spiny Mouse, in response to substrate stiffness. Journal of Biomechanics 2018: **81**: 149–154.

40 Sasaki H, Hokugo A, Wang L *et al.* Neuronal PAS Domain 2 (Npas2)-Deficient Fibroblasts Accelerate Skin Wound Healing and Dermal Collagen Reconstruction. The Anatomical Record 2019: **59**: 340.

41 Phillip J M, Wu P-H, Gilkes D M *et al.* Biophysical and biomolecular determination of cellular age in humans. Nat biomed eng 2017: **1**: 0093.

42 Layton T B, Williams L, Colin-York H *et al.* Single cell force profiling of human myofibroblasts reveals a biophysical spectrum of cell states. Biology Open 2020: **9**: bio049809–14.

43 Hossain M M, Zhao G, Woo M-S *et al.* Deletion of Calponin 2 in Mouse Fibroblasts Increases Myosin II-Dependent Cell Traction Force. Biochemistry 2016: **55**: 6046–6055.

44 Xu J, Nyga A, Li W *et al.* Cobalt ions stimulate a fibrotic response through matrix remodelling, fibroblast contraction and release of pro-fibrotic signals from macrophages. Eur Cell Mater 2018: **36**: 142–155.

45 Reinhart-King C A, Dembo M, Hammer D A. Cell-cell mechanical communication through compliant substrates. Biophysical Journal 2008: **95**: 6044–6051.

46 Califano J P, Reinhart-King C A. Substrate Stiffness and Cell Area Predict Cellular Traction Stresses in Single Cells and Cells in Contact. Cel Mol Bioeng 2010: **3**: 68–75.

47 Tambe D T, Hardin C C, Angelini T E *et al.* Collective cell guidance by cooperative intercellular forces. Nature Materials 2011: **10**: 469–475.

48 Nelson C M, Jean R P, Tan J L *et al.* Emergent patterns of growth controlled by multicellular form and mechanics. Proceedings of the National Academy of Sciences of the United States of America 2005: **102**: 11594–11599.

49 Nelson C M, Pirone D M, Tan J L *et al.* Vascular endothelial-cadherin regulates cytoskeletal tension, cell spreading, and focal adhesions by stimulating RhoA. Mol Biol Cell 2004: **15**: 2943–2953.

50 Butler J, Tolic-Norrelykke I, Fabry B *et al.* Traction fields, moments, and strain energy that cells exert on their surroundings. Am J Physiol Cell Physiol 2002: **282**: C595–605.

51 Borghi N, Lowndes M, Maruthamuthu V *et al.* Regulation of cell motile behavior by crosstalk between cadherin- and integrin-mediated adhesions. Proceedings of the National Academy of Sciences of the United States of America 2010: **107**: 13324–13329.

52 Palchesko R N, Zhang L, Sun Y *et al.* Development of polydimethylsiloxane substrates with tunable elastic modulus to study cell mechanobiology in muscle and nerve. PLoS ONE 2012: **7**: e51499.

53 Wang L, Sun B, Ziemer K S *et al.* Chemical and physical modifications to poly(dimethylsiloxane) surfaces affect adhesion of Caco-2 cells. Journal of biomedical materials research Part A 2010: **93**: 1260–1271.

54 Wen J H, Vincent L G, Fuhrmann A *et al.* Interplay of matrix stiffness and protein tethering in stem cell differentiation. Nature Materials 2014: **13**: 979–987.

55 Mih J D, Sharif A S, Liu F *et al.* A Multiwell Platform for Studying Stiffness-Dependent Cell Biology. PLoS ONE 2011: **6**: e19929.

56 Marinkovic A, Mih J D, Park J A *et al.* Improved throughput traction microscopy reveals pivotal role for matrix stiffness in fibroblast contractility and TGF- responsiveness. AJP-Lung Cellular and Molecular Physiology 2012: **303**: L169–L180.

57 Yeung T, Georges P C, Flanagan L A *et al.* Effects of substrate stiffness on cell morphology, cytoskeletal structure, and adhesion. Cell Motility and the Cytoskeleton 2005: **60**: 24–34.

58 Engler A, Sen S, Sweeney H *et al.* Matrix elasticity directs stem cell lineage specification. Cell 2006: **126**: 677–689.

59 Ye G J C, Aratyn-Schaus Y, Nesmith A P *et al.* The contractile strength of vascular smooth muscle myocytes is shape dependent. Integr Biol (Camb) 2014: **6**: 152.

60 Mierke C T, Kollmannsberger P, Zitterbart D P *et al.* Mechano-coupling and regulation of contractility by the vinculin tail domain. Biophysical Journal 2008: **94**: 661–670.

61 Tse J R, Engler A J. Preparation of Hydrogel Substrates with Tunable Mechanical Properties. Hoboken, NJ, USA: John Wiley & Sons, Inc, 2001.

62 Álvarez-González B, Zhang S, Gómez-González M *et al.* Two-Layer Elastographic 3-D Traction Force Microscopy. Sci Rep 2017: **7**: 39315.

63 Gross W, Kress H. Simultaneous measurement of the Young's modulus and the Poisson ratio of thin elastic layers. Soft Matter 2017: **13**: 1048–1055.

64 Denisin A K, Pruitt B L. Tuning the Range of Polyacrylamide Gel Stiffness for Mechanobiology Applications. ACS Appl Mater Interfaces 2016: **8**: 21893–21902.

65 Bashirzadeh Y, Chatterji S, Palmer D *et al.* Stiffness Measurement of Soft Silicone Substrates for Mechanobiology Studies Using a Widefield Fluorescence Microscope. JoVE 2018:

66 Marinkovic A, Mih J D, Park J-A *et al.* Improved throughput traction microscopy reveals pivotal role for matrix stiffness in fibroblast contractility and TGF-β responsiveness. Am J Physiol Lung Cell Mol Physiol 2012: **303**: L169–L180.

67 Pushkarsky I, Tseng P, Black D *et al.* Elastomeric sensor surfaces for high-throughput single-cell force cytometry. Nat biomed eng 2018: **2**: 124–137.

68 Wang Y L, Pelham R J. Preparation of a flexible, porous polyacrylamide substrate for mechanical studies of cultured cells. Meth Enzymol 1998: **298**: 489–496.

69 Reinhart-King C A, Dembo M, Hammer D A. Endothelial cell traction forces on RGD-derivatized polyacrylamide substrata. Langmuir 2003: **19**: 1573–1579.

70 Hynd M R, Frampton J P, Burnham M-R *et al.* Functionalized hydrogel surfaces for the patterning of multiple biomolecules. Journal of biomedical materials research Part A 2007: **81**: 347–54.

71 Charrier E E, Pogoda K, Wells R G *et al.* Control of cell morphology and differentiation by substrates with independently tunable elasticity and viscous dissipation. Nat Comms 2018: **9**: 449–13.

72 Ribeiro A J S, Ang Y-S, Fu J-D *et al.* Contractility of single cardiomyocytes differentiated from pluripotent stem cells depends on physiological shape and substrate stiffness. Proc Natl Acad Sci U S A 2015: **112**: 12705–12710.

73 Berg I C, Underhill G H. High Throughput Traction Force Microscopy for Multicellular Islands on Combinatorial Microarrays. Bio Protoc 2019: **9**: e3418.

74 Maloney J M, Walton E B, Bruce C M *et al.* Influence of finite thickness and stiffness on cellular adhesion-induced deformation of compliant substrata. Physical Review E 2008: **78**: 041923–15.

75 Park C Y, Zhou E H, Tambe D *et al.* High-throughput screening for modulators of cellular contractile force. Integrative Biology 2015: **7**: 1318–1324.

76 Liu K, Yuan Y, Huang J *et al.* Improved-Throughput Traction Microscopy Based on Fluorescence Micropattern for Manual Microscopy. PLoS ONE 2013: **8**: e70122.

77 Lowe D G. Distinctive image features from scale-invariant keypoints. International journal of computer vision 2004: **60**: 91–110.

78 Holenstein C N, Silvan U, Snedeker J G. High-resolution traction force microscopy on small focal adhesions - improved accuracy through optimal marker distribution and optical flow tracking. Sci Rep 2017: **7**: 41633.

79 Raffel M, Willert C E, Kompenhans J *et al.* Particle Image Velocimetry: A Practical Guide. Springer, 2007.

80 Thielicke W. The Flapping Flight of Birds. 2014:

81 Thielicke W, Stamhuis E J. PIVlab - Towards User-friendly, Affordable and Accurate Digital Particle Image Velocimetry in MATLAB. Journal of Open Research Software 2014: **2**: 1202–10.

82 Tseng Q, Duchemin-Pelletier E, Deshiere A *et al.* Spatial organization of the extracellular matrix regulates cell-cell junction positioning. Proceedings of the National Academy of Sciences 2012: **109**: 1506–1511.

83 Martiel J-L, Leal A, Kurzawa L *et al.* Chapter 15 - Measurement of cell traction forces with ImageJ. In: Paluch EK, ed. Methods In Cell Biology. Academic Press, 2015: 269–287.

84 Biel N M, Santostefano K E, DiVita B B *et al.* Vascular Smooth Muscle Cells From Hypertensive Patient-Derived Induced Pluripotent Stem Cells to Advance Hypertension Pharmacogenomics. Stem Cells Transl Med 2015: **4**: 1380–1390.

Supplemental Files

A. Additional Discussion of Substrate Wrinkling Assay (SWA)

Many methods to quantify "wrinkles" of soft silicone substrates will successfully distinguish contractility of adherent cells. As described in the main text (Section 2.4), quantification of substrate wrinkling can be done by hand, semi-automated (manual thresholding), or fully automated. These example approaches and algorithms are compared in Supplemental Figure I and described in detail below.

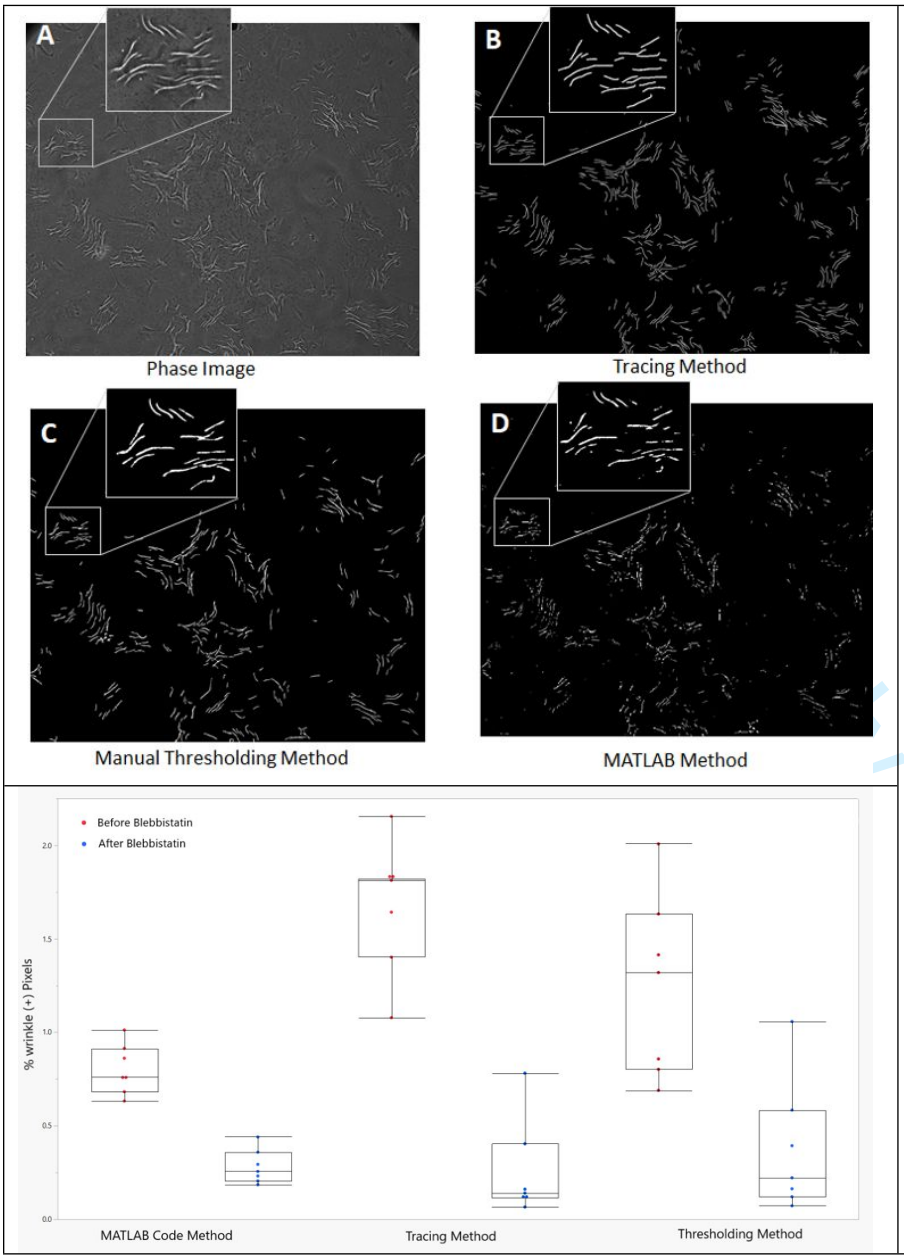

Supplemental Figure I. Example phase contrast image (A) and wrinkle quantification by different methods. (B) Hand tracing method is slow (3-5 mins per image) but robust. (C) Manual thresholding method is quicker (~1 min per image), though it still requires interaction with each image. (D) Fully automated code is rapid (<1 sec per image) but conservative settings to reduce noise may also eliminate some of the signal. Note how some wrinkles appear divided or missing in inset. (E) All three analysis methods detect significant difference between treatments, but the ranges of resulting data vary.

For this example experiment, tissue culture plastic was coated with Sylgard 527 (Dow Corning) per manufacturer's instructions and cured at 70ºC overnight. The plate was plasma-treated for 25 seconds (Harrick Plasma), sterilized under germicidal UV for 1 hour while covered in thin layer of PBS to maintain plasma activation, and coated with collagen I for 45 minutes at 37ºC. After rinsing the surface with sterile saline, passage 3 primary mouse dermal fibroblasts were seeded at a density of ~8,500 cells/cm^2. Once seeded, the cells were allowed to grow to 80% confluency (36-48 hours) before analysis. Seven phase images across two wells were acquired for each condition. Then, the cells were treated with blebbistatin at a concentration of 2.92 µm/ml for 1 hour. Phase images were then taken at the same relative spots as before for comparison.

A.1. Quantifying Wrinkles via ImageJ

Detailed steps for quantifying wrinkles on soft silicone substrates using ImageJ 1.51 on a Mac:

1. Open desired image
2. Using "brush" tool to highlight each wrinkle by hand, zooming in as needed.
    a. *For semi-automation, skip this step.*
3. Threshold the image by selecting Image > Adjust > Threshold
    a. Before thresholding the image, if the image is not 8-bit, convert it by selecting Image > Type > 8-bit.
4. A "Threshold" window will pop up. Using the lower scroll bar, adjust the threshold value until only your wrinkles are visible against the red background (red indicates the area that will be set to black upon thresholding). For manual highlighting, your threshold value will be close to 255; for semi-automated, it will probably be between 100-200. Click "Apply."

Supplemental Figure II.

(a) Original Image

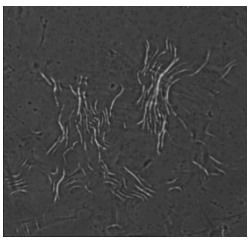

(b) Red highlight while setting threshold (3)

(c) Result after thresholding (4)

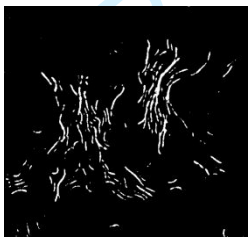

(d) Result after converting to mask (5)

(e) [Left] Dialog window for "Analyze Particles" and [Right] "Bare Outlines" after analyzing particles (6). Note: 10 px was set as minimum size to reduce noise but can be adjusted.

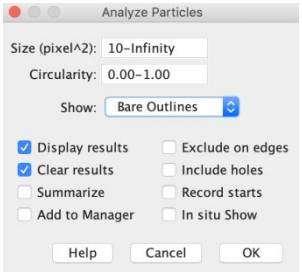

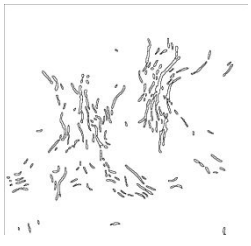

(f) [Left] Dialog box for "Distribution" using wrinkle "Area" as an example and [Right] resulting histogram (7)

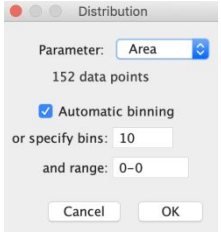

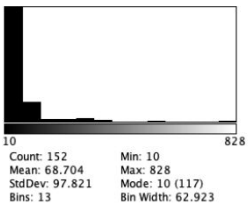

5. Invert colors so that black wrinkles appear against a white background using Process > Binary > Convert to Mask.
6. Executing command Analyze > Analyze Particles will bring up a dialog with choices to filter based on particle size and circularity. To reduce noise, a minimum particle size can be set empirically.
    a. If you have not used this command previously, Analyze > Set Measurements allows you to define measurements of interest. See details at ImageJ website: https://imagej.nih.gov/ij/docs/menus/analyze.html#set
7. From the "Results" window, you can run limited analysis within ImageJ.
    a. Results > Distribution will bring up a dialog box for you to select parameter of interest and bins for a histogram.
    b. Results > Summarize will add basic statistics to your Results window. Note: these statistics will be included in your "Distribution" if you run this step first.
    c. You can also save to an Excel file: File > Save As.

B. Additional Discussion of Quantitative Traction Force Microscopy (qTFM)

B.1. Detailed options for integrating fluorescent markers

In general, a pre-polymer solution is mixed with the desired concentration of fluorescent beads (Figure III.1a) and then sandwiched between two flat surfaces (Figure III.1b). Once polymerized, the coverslip can be removed and the hydrogel functionalized or stored (Figure III.c). *Note:* We have found that level working surfaces are critical to obtaining a flat gel, which is crucial for obtaining in-focus images. Careful practice placing the coverslip flat and leveling all working surfaces helps to obtain a plane of in-focus beads. Take care when working on benchtops covered in absorptive material, and be sure to level surfaces and shelves in relevant equipment.

To reduce noise from out-of-plane beads, a smaller volume of hydrogel mixed with fluorescent beads can placed over a pre-polymerized bead-free hydrogel and covered with a coverslip to create a very thin uniform layer of beads close to the cell-substrate interface (Figure III.2b). In our hands, a concentration of 0.01% of 0.52 μm-diameter beads for the second step of the two-step process produced useful bead densities while limiting clustering. Alternatively, functionalized beads can be bound to the top surface of the functionalized gel without a second gel layer. (1)

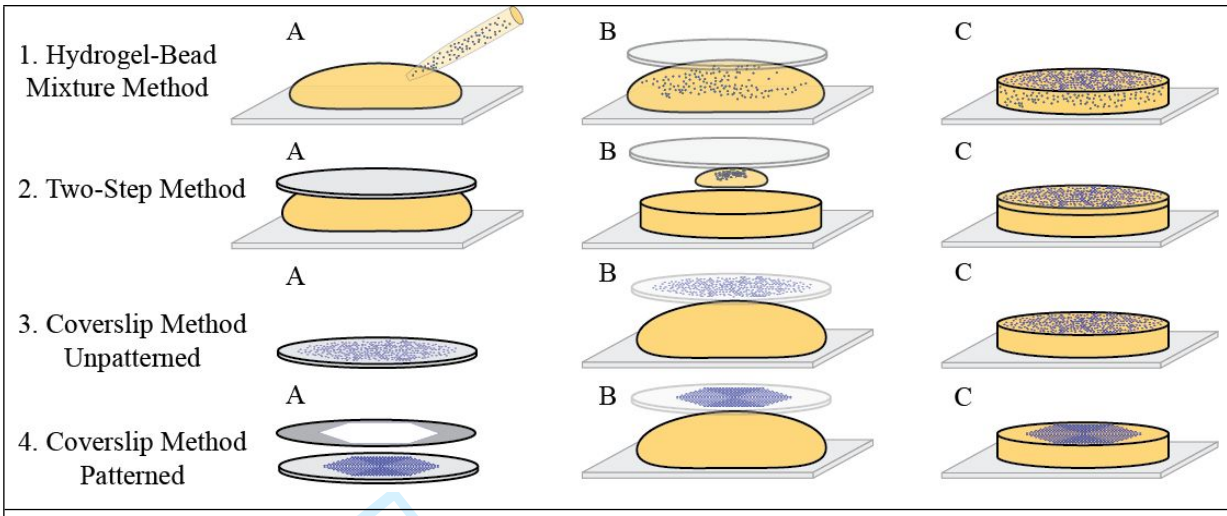

Supplemental Figure III. Methods to fabricate beaded hydrogels. The hydrogel-bead mixture method (1) involves full incorporation of beads into the gel solution. The two-step method (2) involves the polymerization of a "thin" hydrogel (<10 μm) with beads on top of a "thick" substrate (50-150 μm, typically the same hydrogel is used). Alternatively, hydrogels can be polymerized using a coverslip with an unpatterned (3) or patterned (4) bead distribution over the base hydrogel without the need of a second polymerization step.

Other methods for obtaining a planar bead layer include evaporating fluorescent beads onto a coverslip that will serve as the top part of the hydrogel (Figure III.3a). (2) The hydrogel is then sandwiched between the beaded coverslip and another flat surface (Figure III.3b). Once the beaded coverslip is removed, the beads transfer from the coverslip to the hydrogel (III.3c). Coverslip deposition also allows for patterned placement of markers. Printed patterns and soft lithography stamps or stencils can be used to pattern beads onto the coverslip (Figure III.4a), and once the coverslip is removed, the pattern is transferred to the hydrogel (Figure III.4bc). Patterned coverslips can also be used to transfer proteins. (3)

B.2. Biological Considerations of Time-Lapse Experiments

Traction forces may be monitored over extended periods for various applications, for instance, to quantify changes in response to soluble molecules, e.g. growth factors. In addition to maintaining the focal plane, another challenge of long time-lapse experiments include the cells experiencing frequent overexposure to fluorescent wavelengths. This comes from both the excitation wavelength necessary for imaging and the emission wavelength from the fluorescent markers. Exposure of media to fluorescence could also lead to free radical generation and increased toxicity. Therefore, light exposure to the cells and media should be minimized. Phenol-red-free culture media, sodium bicarbonate supplement, HEPES buffer, and frequently changed or perfused media can reduce free radical damage and improve CO2 regulation. Also, pseudo-randomization of the order in which you image samples helps to ensure you are not inadvertently capturing cell response to being on the microscope stage rather than your variables of interest.

B.3. Image Acquisition Parameters and Maintaining Precise Focal Plane

Small drifts in z-plane focus can substantially affect the accuracy of subsequent algorithms. For our setup using 0.52 μm-diameter beads imaged at 200x, we have found that a difference of 1, 2 and 3 μm out-of-focus can create a strain energy percent change of 0.5, 13, and

48%, respectively (Supplemental Figure IV). Strategies to reduce out-of-focus error include upgraded objectives with a small aperture and a large depth of field, implementation of a microscope autofocus system, increased contrast between the beads and the background, creation of a stack in the z-direction to select the best image for each data point, and utilization of larger beads.

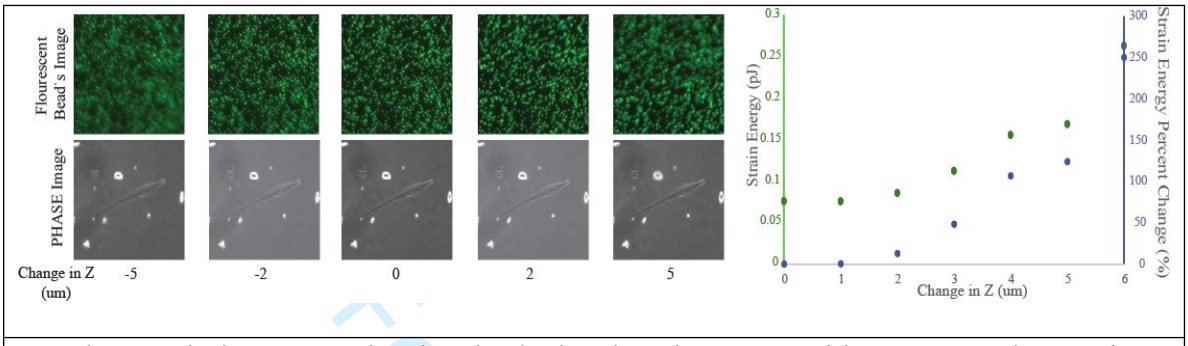

Supplemental Figure IV. Visual and calculated strain energy with respect to changes in the focal layer. Fluorescent and phase-contrast images changes very little from 0 to 2 µm, but a significant visual difference is seen on focal plane differences greater than 4 µm. For 1, 2 and 3 µm out of focus, the strain energy (and percent change) increased from 0.071 pJ to 0.072 pJ (0.5%), 0.090 pJ (12%) and 0.107 pJ (48%), respectively, while for changes greater than 4 µm the strain energy was greater than 0.150 pJ (106%).

B.4. Pre-Processing in PIVlab

In addition to fabrication and experimental techniques to improve signal-to-noise ratio of acquired images, algorithms in *PIVlab* and other software can digitally enhance SNR. In *PIVlab*, contrast limited adaptive histogram equalization (CLAHE) increases readability of image by independently optimizing low and high intensity regions, which improves the detection of displacements. A window size of 10 for the CLAHE filter worked well for our images acquired at 200x magnification (0.16 µm/px) with 0.52 µm beads (Supplemental Figure V). High pass filtering, another option in *PIVlab,* sharpens the image and improves SNR by emphasizing high frequency information and suppressing low frequency information. For our methods, a filter setting of 30 improved SNR and subsequent analyses. For consistency, the same pre-processing settings should be used for each data set, similar to fixing exposure intensity and times for fluorescence imaging.

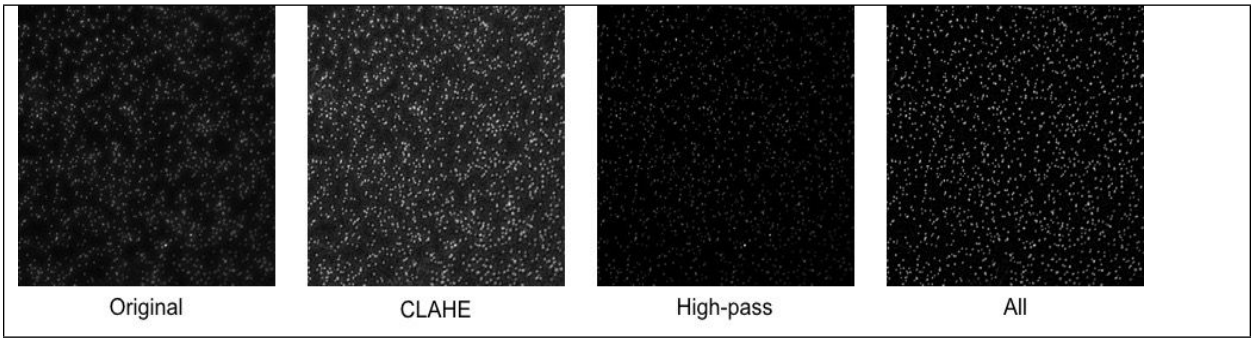

Supplemental Figure V. Effect of image pre-processing techniques in PIVlab. The original image taken at 200x total magnification can be seen after applying contrast limited adaptive histogram equalization (CLAHE), a high pass filter, and both ("All") to the image. The resulting image has improved sharpness and less background noise, which is then used in cross-correlation algorithms to quantify bead displacements.

B.5. Cell-Outline-Based Algorithms for Calculating Contractility

As an alternative to Fourier Transform Traction Cytometry, Boundary-element-based qTFM methods discretize the cell rather than the substrate to calculate traction forces, which requires accurate determination of cell boundaries (4,5). Identification of cell boundary requires a separate image focused on the cell (typically 5-10 µm above the fiducial markers) and can be acquired in phase-contrast or fluorescence. While cell outline algorithms can reduce noise associated with peripheral beads, manual outlining of cells introduces additional variability and increases time-demand, so these algorithms are not recommended for beginners. If using algorithms that require cell outlines, we recommend systematizing identification of cell boundaries to reduce variability, e.g. using fluorescence microscopy (6) or high-resolution phase-contrast microscopy (7).

B.6. Calculating Strain Energy

The total strain energy, W, i.e. work transferred from the cell into the substrate to induce deformations, can be calculated as

$$W = \sum \frac{1}{2} F x^2 \qquad \text{(S1)}$$

where W = strain energy (units: Joules, J), F = force (units: Newtons, N), and x = displacement (units: m). When using ImageJ plugins *PIV* and *FTTC,* the data required for this calculation are stored in two files. The "PIV…" file has relevant displacements (in pixels) and the "Traction…" file has relevant stresses that can be converted to forces.

References

1 Marinkovic A, Mih J D, Park J-A *et al.* Improved throughput traction microscopy reveals pivotal role for matrix stiffness in fibroblast contractility and TGF-β responsiveness. Am J Physiol Lung Cell Mol Physiol 2012: **303**: L169–L180.

2 Simmons C S, Ribeiro A J S, Pruitt B L. Formation of composite polyacrylamide and silicone substrates for independent control of stiffness and strain. Lab Chip 2013: **13**: 646–649.

3 Ribeiro A J S, Ang Y-S, Fu J-D *et al.* Contractility of single cardiomyocytes differentiated from pluripotent stem cells depends on physiological shape and substrate stiffness. Proc Natl Acad Sci U S A 2015: **112**: 12705–12710.

4 Dembo M, Wang Y L. Stresses at the cell-to-substrate interface during locomotion of fibroblasts. Biophysical Journal 1999: **76**: 2307–2316.

5 Munevar S, Wang Y, Dembo M. Traction force microscopy of migrating normal and H-ras transformed 3T3 fibroblasts. Biophysical Journal 2001: **80**: 1744–1757.

6 Arce S H, Wu P-H, Tseng Y. Fast and accurate automated cell boundary determination for fluorescence microscopy. Sci Rep 2013: **3**: 2266–2266.

7 Ambuhl M E, Brepsant C, Meister J J *et al.* High-resolution cell outline segmentation and tracking from phase-contrast microscopy images. Journal of Microscopy 2011: **245**: 161–170.